Self-compression in a multipass cell

GAËTAN JARGOT,1,2,* NOUR DAHER,1 LOÏC LAVENU,1,3 XAVIER DELEN,1 NICOLAS FORGET,2
MARC HANNA,1 AND PATRICK GEORGES1

1Laboratoire Charles Fabry, Institut d'Optique Graduate School, CNRS, Université Paris-Saclay, 91127 Palaiseau Cedex, France
2Fastlite, 165 rue des Cistes Pôle entreprise 95 06600 Antibes, Sophia Antipolis, France
3Amplitude Laser, Cité de la Photonique, 11 avenue de Canteranne, 33600 Pessac, France
*Corresponding author: gaetan.jargot@institutoptique.fr

We demonstrate self-compression of short-wavelength in-frared pulses in a multipass cell (MPC) containing a plate of silica. Nonlinear propagation in the cell in the anomalous dispersion regime results in the generation of 14 μJ22 fs pulses at 125 kHz repetition rate and 1550 nm wavelength. Periodic focusing inside the cell allows us to circumvent catastrophic self-focusing, despite an output peak power of 440 MW well beyond the critical power in silica of 10 MW. This technique allows straightforward energy scal-ing of self-compression setups and control over the spatial manifestation of Kerr nonlinearity. More generally, MPCs can be used to perform, at higher energy levels, temporal manipulations of pulses that have been previously demon-strated in waveguides.

Ultrafast lasers have allowed a plethora of applications, ranging from industrial processing to a large number of scientific advances such as multiphoton imaging, ultrafast dynamics studies, and strong field physics. In the short-wavelength infrared (SWIR) and mid-infrared (MIR) wavelength ranges, applications such as high-harmonic generation in gases [1], solids [2], and multidimensional molecular spectroscopy [3] are pushing the development of high-power microjoule–millijoule laser systems with pulse durations in the few-cycle regime. In this wavelength range, the most widespread sources of ultrashort pulses are optical parametric chirped pulse amplifiers (OPCPAs) that readily deliver pulses with sub-100 fs durations at high repetition rates [4–8].

Access to shorter pulse durations is often allowed by implementing a nonlinear compression setup at the output of the laser system. Propagation of the pulse in a solid or gas material induces spectral broadening through self-phase modulation (SPM), corresponding to a shorter Fourier-transform limited pulse. For sources in the near-infrared, where material dispersion is normal, additional negative dispersion must be added after the SPM stage [9]. For sources in the SWIR and MIR, most optical materials exhibit anomalous dispersion, and soliton dynamics results in compression in the initial stage of propagation. Although self-compression can be performed in gaseous [10] and bulk solid [11] media, these experiments often show low energy transfer to the compressed pulse and more difficult experimental control because of the complex spatio-temporal dynamics. Alternatively, the use of a waveguide allows large interaction lengths and negates the spatial Kerr effect, resulting in efficient and well-controlled setups. Energy scaling in waveguides is challenging, requiring, for instance, the use of gas-filled anti-resonant photonic crystal fiber designs to increase the critical power for self-focusing, ensure low losses, and induce anomalous dispersion [12].

Recently, a concept allowing the use of a bulk nonlinear medium while retaining the advantages of waveguides has emerged [13]. It consists of placing the nonlinear medium inside a multipass cell (MPC) and accumulating the nonlinearity over a large number of passes, so that nonlinear propagation in the medium can be seen as a small perturbation to free-space propagation as far as spatial effects are concerned. This can be compared to waveguides where spatial nonlinear effects change slightly the mode structure [14] without significant physical impact. It can also be considered as an extension of multi-plate setups [15–17] with a distribution of the nonlinearity over tens of passes in the material instead of a few. Although it was proposed as early as 2000 [18], it is only recently that this idea has been demonstrated [13].

The concept was first implemented with a solid nonlinear medium [13,19,20], where it was shown that the peak power can exceed the critical power in the medium without affecting the spatial profile at the output. The MPC idea was then used with a gas medium [21,22], at higher energy levels of 140 μJ and 2 mJ, respectively. These demonstrations have all been done in setups where the net dispersion in the MPC was either negligible or slightly normal, resulting in an essentially stationary temporal profile during propagation and necessitating negative dispersion at the output to compress the pulse.

Here we report the use of an MPC in net anomalous dispersion regime to take advantage of soliton dynamics and self-compress 19 μJ 63 fs pulses generated by an OPCPA at 1.55 μm down to a 22 fs pulse duration with a transmission of 73%. The experimental data are compared to a 3D numerical model, and the output beam is characterized in terms of spatio-spectral couplings. This experiment establishes the use of MPCs as a simple way to scale the energy of nonlinear

functions usually performed in waveguides, essentially opening ultrafast nonlinear fiber optics to higher pulse energies.

Figure 1 depicts the SWIR OPCPA operated at 125 kHz and 1550 nm that follows the overall architecture reported in Ref. [7], with some modifications. The setup is based on a femtosecond ytterbium-doped fiber amplifier system (Tangerine, Amplitude Systèmes) that delivers 400 μJ 400 fs pulses at a 125 kHz repetition rate with a central wavelength at 1030 nm. A small fraction (4 μJ) of the pump beam is used to generate a stable seed extending from 1300 to 1700 nm through supercontinuum generation in a 10 mm long YAG crystal [23]. This signal is temporally stretched by passing through 3 mm of silicon in order to reach the best trade-off between the gain and bandwidth in the first parametric amplification stage, carried out in a 1 mm long Mgo:PPLN fanout crystal. At the output of this stage, pumped with 13 μJ, the signal energy is 500 nJ, with a spectrum centered at 1550 nm. After propagation through 2 mm of additional silicon, the signal is sent to the second and last stage of parametric amplification, based on a 3 mm long KTA crystal used in type II non-collinear phase matching. The signal pulses are amplified to 22.5 μJ. Compression is achieved by propagation in 210 mm of silica, with a transmission of 86%. The compressed pulse energy is 19 μJ, corresponding to 2.4 W average power.

The OPCPA output properties are shown in Fig. 2. The temporal profile and spectrum are measured with a second-harmonic generation frequency-resolved optical gating (FROG) apparatus. The full width at half-maximum (FWHM) pulse duration is 63 fs, with a 120 nm bandwidth at −10 dB. The spatial beam profile is measured using an InGaAs camera, showing a slightly elliptic beam, as shown in the inset Fig. 2(a).

In optical fibers, soliton dynamics in the anomalous dispersion regime induces self-compression for soliton number $N = \sqrt{L_d/L_{\mathrm{SPM}}} > 1$, where $L_d = T_0^2/\beta_2$ is the dispersion length, T_0 is the input pulse duration, and β_2 is the group-velocity dispersion. The characteristic length for SPM is $L_{\mathrm{SPM}} = cA_{\mathrm{eff}}/\omega_0 n_2 P_{\mathrm{peak}}$, where c is the speed of light, A_{eff} is the effective area, ω_0 is the optical angular frequency, n_2 is the nonlinear index, and P_{peak} is the input peak power. In order to keep a clean compressed pulse, small values of N are required ($N \leq 5$), since larger values of N result in a reduced fraction of energy contained in the compressed temporal feature at the output. The compression ratio and optimal compression distance are found to scale like N and $1/N$, respectively [24]. Deviations from these scaling laws depend on the influence of higher-order effects such as higher-order dispersion and self-steepening.

Here we use an MPC that includes a 2 mm plate of anti-reflection coated (1300–1700 nm) silica to perform self-compression. The output beam from the OPCPA is coupled in and out of the MPC using rectangular-shaped mirrors (3 mm × 10 mm) located in front of one of the MPC mirrors. These mirrors (Layertec coating 113504) have a diameter of 25.4 mm and a radius of curvature of 200 mm, and are coated to be highly reflective (>99.8%) in the 1400–1700 nm range while introducing low group delay dispersion. The MPC is 280 mm long, and the silica plate is located asymmetrically at a distance of 100 mm from one of the MPC mirror. This adjustment is an experimentally convenient way to tune the level of nonlinearity, since the beam width increases from the MPC center to the mirrors. Stationary beam propagation in this MPC requires a beam radius at $1/e^2$ of 212 μm at the MPC waist, expanding to 388 μm radius at the MPC mirrors. Experimentally, an arrangement of two lenses with a focal length $f = 150$ mm and $f = -100$ mm at the input of the cell allows us to match this value, with a measured radius of 225 × 270 μm. At the output of the MPC, the beam is collimated with a $f = 750$ mm

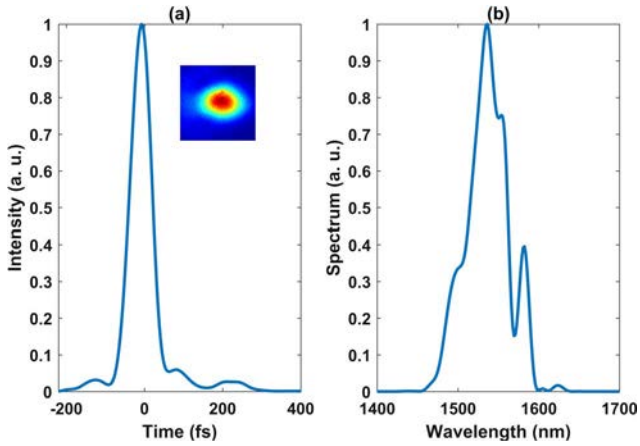

Fig. 2. (a) Temporal profile at the output of the OPCPA. Inset: spatial profile. (b) Spectrum at the OPCPA output. The FROG error is 61 × 10^{-4} on a 256 × 256 grid.

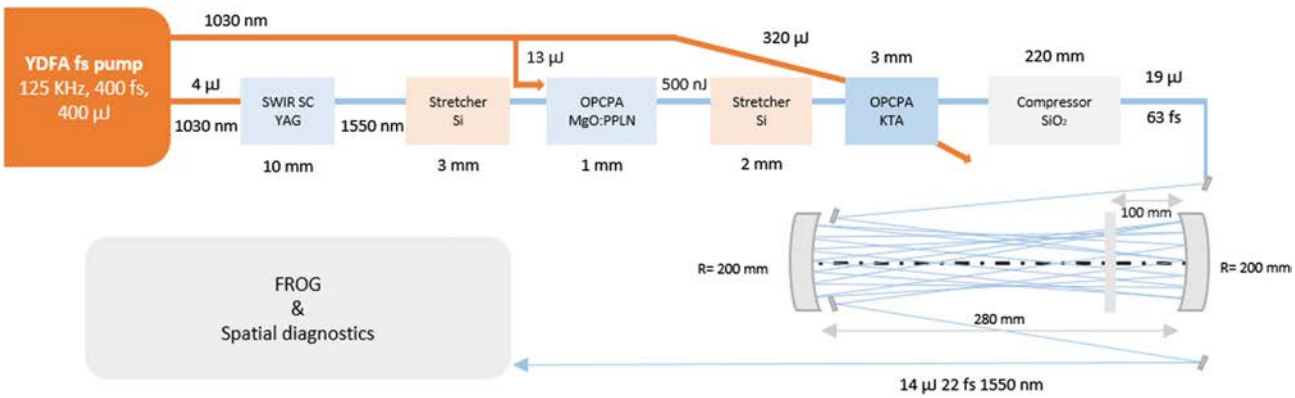

Fig. 1. Experimental setup.

lens, and silver-protected mirrors are used to route it to diagnostics.

In terms of soliton parameters, using the input pulse parameters from the OPCPA, the dispersion and nonlinear index of silica at 1550 nm $\beta_2 = -28$ fs^2/mm and $n_2 = 2.7 \times 10^{-20}$ m^2/W, this MPC geometry translates in $L_D = 45$ mm and $L_{\mathrm{NL}} = 5.9$ mm, giving a soliton parameter $N = 2.7$. The most obvious deviations from the theoretical soliton framework are the spatial imperfections that are not present in a single-mode optical fiber, and the introduction of higher-order dispersion and spectral filtering at the mirrors. This dispersion results in a net zero dispersion wavelength shifted from 1300 nm for pure silica to 1450 nm for the MPC, so that the spectral content generated below this value will not participate further in the soliton dynamics.

The position and orientation of the input and output coupling mirrors allow us to select the number of roundtrips in the MPC. They are adjusted to make 10 roundtrips, resulting in an overall propagation distance in the silica of 40 mm. Figure 3 shows the measured and retrieved FROG traces and the related temporal profile and spectrum, when the input pulse energy is 19 μJ, without any additional dispersion added between the MPC and diagnostics. The FWHM pulse width is 22 fs, corresponding to a compression ratio of 2.8. The spectrum extends over the full bandwidth of the mirrors from 1300 to 1700 nm, with a bandwidth at −10 dB of 310 nm corresponding to a Fourier transform-limited pulse duration of 20 fs. The energy

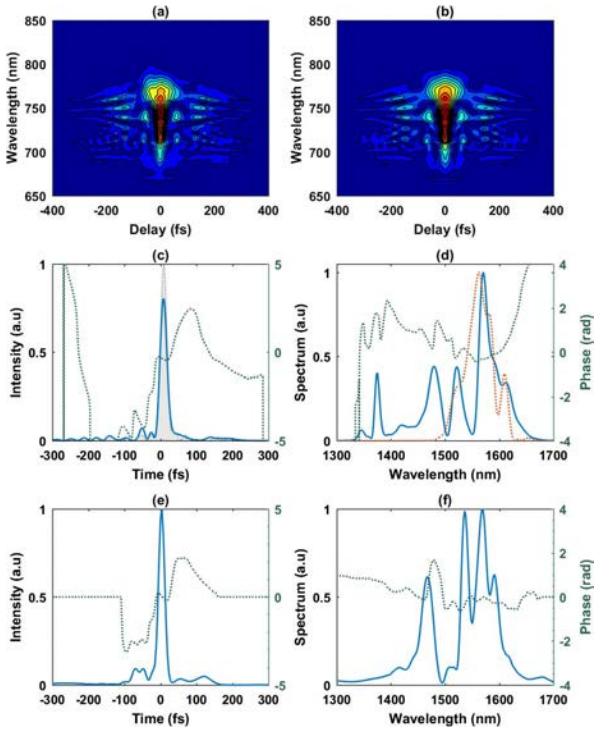

Fig. 3. (a) Measured and (b) retrieved FROG traces at the output of the compression setup at maximum input energy of 19 μJ. The FROG error is 57×10^{-4} on a 256×256 grid. (c) FROG-retrieved temporal profile (blue), temporal phase profile (dashed green), and Fourier transform-limited profile (gray) compared to (e) the numerical model. (d) FROG-retrieved spectrum (solid blue), spectral phase profile (dashed green), and initial OPCPA spectrum (dashed red) compared to (f) the numerical model.

transmission of the MPC starts at 80% at low input energy, and drops down to 73% at the highest energy of 19 μJ, resulting in 14 μJ output pulses. This drop can be confidently attributed to the mirror bandwidths that are not able to reflect the full spectral content generated through soliton compression. The estimated peak power using the measured temporal profile and energy at the output is 440 MW, 40 times higher than the critical power in bulk silica. This highlights the main advantage of this geometry, first pointed out in Ref. [13]: it allows nonlinear propagation over an accumulated distance that is greater than the self-focusing distance (estimated to 15 mm in this experiment) in the material, with minor impact on the spatial profile, as will be described hereafter.

Numerical simulations are performed to ensure that the physics underlying the compression is well captured by a 3D model based on an envelope equation described in Ref. [25], solved using the split-step method described in Ref. [26]. This model includes self-steepening, in addition to diffraction, dispersion to all orders, and instantaneous Kerr effect. The mirror dispersion and reflection curves are fitted to the supplier data to account for this deviation from the ideal soliton model. The temporal initial condition is taken from the FROG–retrieved field at the output of the OPCPA. The input spatial profile is a perfect Gaussian function that matches the stationary MPC beam. The input energy is adjusted to 12 μJ to match the experimentally obtained optimal compression point of 10 roundtrips. This discrepancy is most probably due to the non-perfect spatial quality and mode matching which translate into an experimentally lower level of nonlinearity. The simulated temporal profile and spectrum are plotted along with the experimental results in Fig. 3, and show qualitative agreement. However, the exact spectral structure is not reproduced accurately. This could be due to a number of reasons, including uncertainty in the dispersion profile of the mirror coatings, a non-perfect spatial profile in the experiment, or the fact that air was not included in the simulation as a dispersive and nonlinear medium. The on-axis B-integral per pass through the silica plate grows from 0.4 to 1 rad because of the self-compressing temporal profile, with an integrated value of 13.5 rad. This model also allows us to point out what limits the pulse duration in the current experiment: if the realistically dispersive and filtering mirrors are replaced with dispersionless infinitely broadband mirrors, compression down to sub −10 fs (two optical cycles at 1550 nm) should be achievable.

We now focus on the spatial properties of the output beam, of particular importance in MPC-based nonlinear optics setups. The M^2 parameter is measured at the output of the MPC using a lens and InGaAs camera, both in linear (low energy) and nonlinear (full energy) propagation regimes. The collimated spatial beam profile is observed to slightly decrease in size as the energy is increased, an effect also observed in simulations. However, as shown in Fig. 4, the spatial quality remains essentially constant with M^2 values of 1.53×1.15 at low power going to 1.49×1.24 at the highest energy.

We also assess the spatio-spectral homogeneity by measuring the spectral content at different locations in the compressed output beam. This is an important point to assess the MPC-induced spatial homogenization of nonlinearities. A multimode fiber with a 200 μm core is translated into the output beam and coupled to a spectrometer. The result of this measurement is plotted in Fig. 4. The plotted quantity is the spectral overlap

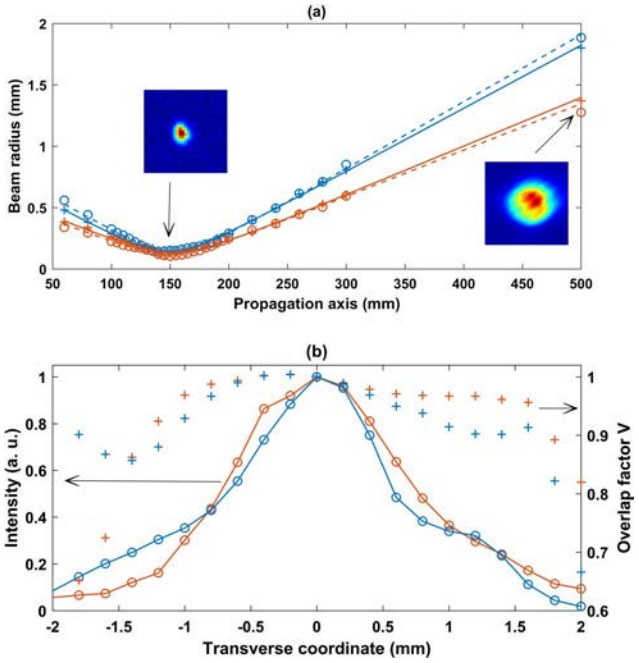

Fig. 4. (a) M^2 measurements of the output beam at low energy (dashed line) and at full energy (solid line) in the horizontal (blue) and vertical (red) directions. (b) Spectral overlap factor with a beam center and intensity as a function of horizontal (blue) and vertical (red) transverse dimensions.

with the beam center [19] that remains above 90% in the central part of the beam. It decreases to lower values at intensity points below 10% of the maximum value. We attribute this decrease to both a decreasing signal-to-noise ratio that artificially degrades the overlap and to a halo that is present in the input beam that is not compressed in the MPC. The mean value of the spectral overlap over the entire beam is 93%, to be compared with a value of 99% in simulations. Again, the input spatial imperfections might explain this discrepancy. Overall, the spatial and spatio-temporal quality at the output is well controlled.

To conclude, we demonstrate for the first time, to the best of our knowledge, self-compression of ultrashort pulses in the SWIR using an MPC setup. This results in the generation of 14 μJ 22 fs output pulses at 125 kHz. This experiment establishes MPCs as a general nonlinear optics tool that allows retaining temporal nonlinearities while homogenizing the spatial Kerr effect. It also allows straightforward energy scaling by adjusting the MPC geometry, mirrors, and nonlinear material to fit the input pulse characteristics. Mirror coating technology is crucial to allow high energy transmission and access to the few-cycle regime, and limits the pulse duration in this demonstration. These coatings can be engineered to introduce a net anomalous dispersion in the cell so that self-compression can be achieved in a large variety of media (gases, solids) and wavelength ranges. We believe that MPCs with advanced mirror designs will allow the scaling of self-compression setups to high energy and few-cycle pulses in a robust experimental setup. This should enable applications in the SWIR and MIR wavelength range, and we more generally expect the number of nonlinear MPC applications to grow, since it constitutes a unique tool in the current ultrafast technology landscape.

Funding. Agence Nationale de la Recherche (ANR) (ANR-10-LABX-0039-PALM, ANR-16-CE30-0027-01); Conseil Départemental de lapos'Essonne (Sophie).

REFERENCES

1. T. Popmintchev, M.-C. Chen, D. Popmintchev, P. Arpin, S. Brown, S. Ališauskas, G. Andriukaitis, T. Balčiunas, O. D. Mücke, A. Pugzlys, A. Baltuška, B. Shim, S. E. Schrauth, A. Gaeta, C. Hernández-García, L. Plaja, A. Becker, A. Jaron-Becker, M. M. Murnane, and H. C. Kapteyn, Science **336**, 1287 (2012).
2. S. Ghimire, A. D. DiChiara, E. Sistrunk, P. Agostini, L. F. DiMauro, and D. A. Reis, Nat. Phys. **7**, 138 (2011).
3. B. M. Luther, K. M. Tracy, M. Gerrity, S. Brown, and A. T. Krummel, Opt. Express **24**, 4117 (2016).
4. N. Thiré, R. Maksimenka, B. Kiss, C. Ferchaud, P. Bizouard, E. Cormier, K. Osvay, and N. Forget, Opt. Express **25**, 1505 (2017).
5. M. Neuhaus, H. Fuest, M. Seeger, J. Schötz, M. Trubetskov, P. Russbueldt, H. D. Hoffmann, E. Riedle, Z. Major, V. Pervak, M. F. Kling, and P. Wnuk, Opt. Express **26**, 16074 (2018).
6. M. Mero, F. Noack, F. Bach, V. Petrov, and M. J. J. Vrakking, Opt. Express **23**, 33157 (2015).
7. P. Rigaud, A. V. de Walle, M. Hanna, N. Forget, F. Guichard, Y. Zaouter, K. Guesmi, F. Druon, and P. Georges, Opt. Express **24**, 26494 (2016).
8. O. Chalus, P. K. Bates, M. Smolarski, and J. Biegert, Opt. Express **17**, 3587 (2009).
9. W. J. Tomlinson, R. H. Stolen, and C. V. Shank, J. Opt. Soc. Am. B **1**, 139 (1984).
10. A. V. Mitrofanov, A. A. Voronin, M. V. Rozhko, D. A. Sidorov-Biryukov, A. B. Fedotov, A. Pugžlys, V. Shumakova, S. Ališauskas, A. Baltuška, and A. M. Zheltikov, Optica **4**, 1405 (2017).
11. D. Majus, G. Tamošauskas, I. Gražulevičiūtė, N. Garejev, A. Lotti, A. Couairon, D. Faccio, and A. Dubietis, Phys. Rev. Lett. **112**, 193901 (2014).
12. U. Elu, M. Baudisch, H. Pires, F. Tani, M. H. Frosz, F. Köttig, A. Ermolov, P. St.J. Russell, and J. Biegert, Optica **4**, 1024 (2017).
13. J. Schulte, T. Sartorius, J. Weitenberg, A. Vernaleken, and P. Russbueldt, Opt. Lett. **41**, 4511 (2016).
14. L. Dong, J. Lightwave Technol. **26**, 3476 (2008).
15. F. Lu, P. Xia, Y. Matsumoto, T. Kanai, N. Ishii, and J. Itatani, Opt. Lett. **43**, 2720 (2018).
16. J. E. Beetar, S. Gholam-Mirzaei, and M. Chini, Appl. Phys. Lett. **112**, 051102 (2018).
17. M. Seidel, G. Arisholm, J. Brons, V. Pervak, and O. Pronin, Opt. Express **24**, 9412 (2016).
18. N. Milosevic, G. Tempea, and T. Brabec, Opt. Lett. **25**, 672 (2000).
19. J. Weitenberg, A. Vernaleken, J. Schulte, A. Ozawa, T. Sartorius, V. Pervak, H.-D. Hoffmann, T. Udem, P. Russbüldt, and T. W. Hänsch, Opt. Express **25**, 20502 (2017).
20. K. Fritsch, M. Poetzlberger, V. Pervak, J. Brons, and O. Pronin, Opt. Lett. **43**, 4643 (2018).
21. L. Lavenu, M. Natile, F. Guichard, Y. Zaouter, X. Delen, M. Hanna, E. Mottay, and P. Georges, Opt. Lett. **43**, 2252 (2018).
22. M. Ueffing, S. Reiger, M. Kaumanns, V. Pervak, M. Trubetskov, T. Nubbemeyer, and F. Krausz, Opt. Lett. **43**, 2070 (2018).
23. A. van de Walle, M. Hanna, F. Guichard, Y. Zaouter, A. Thai, N. Forget, and P. Georges, Opt. Lett. **40**, 673 (2015).
24. G. Agrawal, *Nonlinear Fiber Optics* (2007).
25. T. Brabec and F. Krausz, Phys. Rev. Lett. **78**, 3282 (1997).
26. M. Hanna, X. Délen, L. Lavenu, F. Guichard, Y. Zaouter, F. Druon, and P. Georges, J. Opt. Soc. Am. B **34**, 1340 (2017).